

Five-institution study of automated classification of pathological slowing from adult scalp electroencephalograms

Wei Yan Peh¹, John Thomas¹, Elham Bagheri¹, Rima Chaudhari², Sagar Karia³, Rahul Rathakrishnan⁴, Vinay Saini⁵, Nilesh Shah³, Rohit Srivastava⁵, Yee-Leng Tan⁶, and Justin Dauwels^{1**}

¹*Nanyang Technological University, Singapore*

²*Fortis Hospital Mulund, Mumbai, India*

³*Lokmanya Tilak Municipal General Hospital, India*

⁴*National University Hospital, Singapore*

⁵*Department of Biosciences and Bioengineering, IIT Bombay, India*

⁶*National Neuroscience Institute, Singapore*

Pathological slowing in the electroencephalogram (EEG) is widely investigated for the diagnosis of neurological disorders. Currently, the gold standard for slowing detection is the visual inspection of the EEG by experts. However, visual inspection is time-consuming and subjective. Moreover, there is shortage of EEG experts worldwide. To address those issues, we propose three automated approaches to detect slowing in EEG: unsupervised learning system (ULS), supervised shallow learning system (SSLS), and supervised deep learning system (SDLS). These systems are evaluated on single-channel segments (channel-level), multi-channel segments (segment-level), and entire EEGs (EEG-level). The ULS performs prediction via spectrum features. By contrast, the SSLS and SDLS detect slowing at individual channels, and those detections are arranged in histograms for detection of slowing at the segment- and EEG-level. We evaluate the systems through Leave-One-Subject-Out (LOSO) cross-validation (CV) and Leave-One-Institution-Out (LOIO) CV on four datasets from the US, Singapore, and India. The SDLS achieved the best overall results: LOIO CV mean balanced accuracy (BAC) of 71.9%, 75.5%, and 82.0% at channel-, segment- and EEG-level, and LOSO CV mean BAC of 73.6%, 77.2%, and 81.8% at channel-, segment-, and EEG-level. The channel- and segment-level performance is comparable to the intra-rater agreement (IRA) of an expert of 72.4% and 82%. The SDLS can process a 30-minutes EEG in 4 seconds, and may be deployed to assist clinicians in interpreting EEGs.

Keywords: Pathological slowing; Electroencephalogram; EEG classification; Slowing detection; Deep learning; Multi-center study.

1. Introduction

Slowing in electroencephalogram (EEG) is an indication of potential neurological dysfunctions such as epilepsy, stroke, or dementia.¹⁻⁴ An abnormal amount of slowing in EEG suggests neurological abnormalities or poor prognosis for neurological recovery. The severity of slowing is dependent on EEG frequency (delta or theta), duration (persistent or intermittent), and location of the slowing (focal or

generalized).⁴ Slow waves can appear in the delta and theta frequency band, with delta slowing exhibiting a more severe pattern of slowing.⁵

Persistent slowing is present in at least 50% of the EEG recording, while intermittent slowing is present between 11% to 49% of the EEG recording.^{6,7} Meanwhile, generalized slowing occurs throughout the brain, whereas focal slowing occurs only in one brain region.³ Generalized and persistent

*Corresponding author, Email: jdauwels@ntu.edu.sg

slowing often leads to a poorer prognosis for recovery. However, slowing can be a normal EEG characteristic, such as in the elderly as slow background or Posterior Slow Waves of Youth (PSWY) in adolescence.⁸ Hence, the classification of pathological slowing can be challenging.

In current clinical practice, the gold standard for slowing annotation in EEG is through visual inspection by neurologists. This can be a time-consuming process. Slowing annotation can be strenuous due to the variation in the slowing duration and location. Furthermore, if a more prominent EEG event is detected (such as a seizure onset), slowing may be less emphasized or given less weightage in the clinical report. Moreover, if Magnetic Resonance Imaging (MRI) or other imaging modalities are available, EEG slowing may become less relevant for diagnosis.⁹ In this case, slowing may not be mentioned in the clinical report at all. Therefore, the reporting of slowing in the clinical report may not always be reliable nor consistent. While imaging techniques may render slowing in EEG less clinically relevant, there are situations where they are unavailable, and EEG is the primary diagnostic tool (e.g., for fast triage in emergency responses, or in local clinics that do not have access to MRI scanners).

As far as we know, no studies so far have investigated how to directly detect slowing from EEG in an automated manner. Instead, existing methods aim to detect neurological disorders from EEG that exhibit slowing (such as stroke, brain injury, seizures), without detecting EEG slowing explicitly.^{10–14} Spectral features are widely applied for such analysis as they are scale-invariant (independent of amplitude or power).¹⁵ For EEG classification, the methods adopted are simple thresholding, traditional machine (shallow) learning, or deep learning via Convolutional Neural Networks (CNN).^{1, 16–19} One drawback of most CNN approaches is that they only investigate single-channel EEG, or only assess the CNNs on a small set of multi-channel EEGs from a single institution.^{18, 20–23} Additionally, current approaches do not explicitly detect pathological slowing. Instead, they classify EEGs with neurological conditions directly.^{24, 25}

An abnormal quantity of slowing in EEG provides information to diagnose a neurological disorder and prescribe an appropriate and timely treatment. For instance, brain tumors may be associated with

localized and persistent EEG slowing.²⁶ Hence, identifying brain regions that exhibit that type of slowing may help confirm or better localize brain tumors. Consequently, there is a demand for automated EEG classification systems that detect abnormal slowing in EEGs for a more reliable diagnosis. To address these shortcomings, we design three automated systems to detect pathological slowing and evaluated the systems on EEGs from multiple institutions in Singapore, India, and the US.

In this paper, we proposed three automated systems for detecting pathological slowing in EEG (see Table 1): unsupervised learning system (ULS), supervised shallow learning system (SSLS), and supervised deep learning system (SDLS). The systems detect pathological slowing at single-channel EEG segments (channel-level), multi-channel segments (segment-level), and full EEGs (EEG-level), allowing us to detect slowing at all scales (see Figure 1). The ULS performs segment- and EEG-level classification without a supervised channel-level EEG slowing detector by assessing the EEG spectral distributions. By contrast, the SSLS and SDLS perform the classification in two stages. The first stage deploys a supervised shallow or deep learning-based slowing detector to detect slowing at the channel-level. The second stage utilizes the channel-level detections to identify pathological slowing in EEG segments or full EEGs.

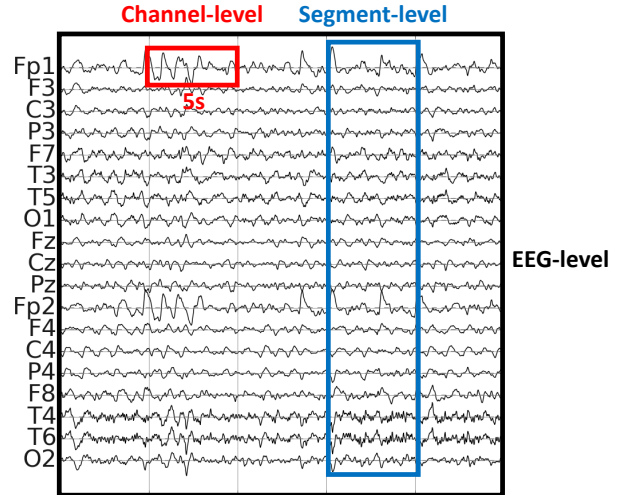


Figure 1. Channel-, segment- and EEG-level.

The ULS was designed as a benchmark to assess the improvement afforded by a system with a supervised channel-level slowing detector. Meanwhile, we implemented a shallow and deep learning model for

the channel-level slowing detector to quantify the advantages of deep learning. To the best of our knowledge, this current study is the first to design channel-, segment-, and EEG-level classification systems. Additionally, this study is the first to detect pathological slowing in EEG without any information on the neurological disorder. As far as we know, all prior studies concentrate on detecting neurological disorders from EEG that cause EEG slowing, but do not directly detect slowing.

We validate the performance of the proposed systems on multiple datasets by considering two real-world scenarios. In the first scenario, we assume to have access to some past EEGs (around 50 to 100 EEGs) and their clinical reports. With the data, we can retrain the classification system to perform predictions on EEGs from that center in the future. To assess the performance of the system in this scenario, we apply Leave-One-Subject-Out (LOSO) cross-validation (CV) for each institute (dataset) separately. In LOSO CV, we select one subject for testing and the remaining subjects to train the classification system. We repeat this for each subject and compute the performance of the systems across all the subjects.

In the second scenario, we assume that no EEGs nor clinical reports are available from the new center for calibration. Instead, we utilize existing datasets to train the classification system to predict the labels of those EEGs from the new center. We evaluate our proposed systems under this scenario by Leave-One-Institution-Out (LOIO) CV. First, we select an institute of our pool of participating institutes (cf. Section 2.1) and leave it out for testing. The EEGs from the remaining institutes are employed to train the classification system. We repeat this for each institution.

To the best of our knowledge, this current study is the first to perform a cross-institutional assessment of automated EEG classification systems to detect pathological slowing. It is crucial to perform the LOIO CV assessment to evaluate the generalizability of the proposed system. Similarly, we perform the LOSO CV assessment to evaluate the proposed classification systems after recalibration for a particular dataset.

As our results show, the SDLS achieves the best overall performance for the three classification tasks. It yields an LOIO CV mean balanced accu-

racy (BAC) of 71.9%, 75.5%, and 82.0%, for the channel-, segment- and EEG-level classification, respectively, whereas the LOSO CV mean BAC are 73.6%, 77.2%, and 81.8%, respectively. The channel- and segment-level intra-rater agreement (IRA) of an expert is 72.4% and 82% respectively on the same data. Thus, the SDLS can detect abnormal slowing in channels and segments reliably at the level of the human expert. Moreover, the SDLS can process a 30-minute EEG in about 4 seconds. Therefore, the proposed systems for automated detection of EEG slowing might be useful in clinical applications.

The rest of this paper is organized as follows. In Section 2.1, we describe the EEG datasets and the preprocessing steps employed in this study. In Section 2.2, we review various spectral features considered in this study, while in Section 2.3, we describe the EEG channel and segment datasets. In Section 2.4, we present the three proposed machine learning systems for channel-, segment-, and EEG-level slowing detection. In Section 3, we show numerical results for the different classification systems and tasks, while in Section 4, we discuss the performance of the proposed systems and their potential relevance in clinical practice. Lastly, in Section 5, we offer concluding remarks and suggestions for future work.

2. Materials and Methods

2.1. Scalp EEG dataset

We analyzed scalp EEG recording from five institutions:

- (1) Temple University Hospital (TUH), USA.
- (2) National Neuroscience Institute (NNI), Singapore.
- (3) National University Hospital (NUH), Singapore.
- (4) Fortis Hospital, Mumbai, India.
- (5) Lokmanya Tilak Municipal General Hospital (LTMGH), Mumbai, India.

The review boards of the respective institutions have approved this study. The EEGs were recorded by 19 electrodes placed according to the International 10-20 System. The datasets predominantly consist of awake adult EEGs (age \geq 18 years). We have access to the EEGs and their clinical reports, except for the NUH dataset. Hence, we cannot perform EEG-level classification as we have no access to information about slowing in the NUH dataset.

Table 1. Summary of the three EEG classification system.

Classification System	Channel-Level Slow Detection	Segment- or EEG-Level Slow Detection
Unsupervised Learning System (ULS)	<ul style="list-style-type: none"> • Features: Spectral features • Classifier: Simple thresholding • Comments: Segment- and EEG-level slowing detection does not rely on channel-level slowing detection. We introduced simple thresholding as a simple channel-level classifier for illustration purposes 	<ul style="list-style-type: none"> • Features: Histogram-based features* of the spectral measures computed from 5s single-channel segments (with 75% overlap) • Segment/EEG Classifier: Shallow learning model
Supervised Shallow Learning System (SSLS)	<ul style="list-style-type: none"> • Features: Spectral features • Classifier: Shallow learning model 	<ul style="list-style-type: none"> • Features: Histogram-based features* of channel-level detector outputs computed from 5s single-channel segments (with 75% overlap) • Segment/EEG Classifier: Shallow learning model
Supervised Deep Learning System (SDLS)	<ul style="list-style-type: none"> • Features: EEG spectrum • Classifier: Deep learning model (CNN) 	<ul style="list-style-type: none"> • Features: Histogram-based features* of channel-level detector outputs computed from 5s single-channel segments (with 75% overlap) • Segment/EEG Classifier: Shallow learning model

* Histogram counts, in addition to the mean, median, mode, standard deviation (std), minimum value, maximum value, range, kurtosis, and skewness.

If an EEG report mentions abnormal slowing, we assume that the corresponding EEG indeed contains pathological slowing; otherwise, the EEG is considered free of slowing. The proposed EEG-level classifiers aim to predict whether pathological slowing is mentioned in the clinical report for an EEG. The details of the EEG datasets are tabulated in Table 2.

The TUH dataset is the largest public epilepsy EEG dataset. Concretely, we investigate two corpora from the TUH dataset: TUH Slowing Corpus and TUH Abnormal Corpus.^{24,27,28} The NNI, Fortis, and NUH datasets consist of scalp EEGs recorded during routine clinical care. However, the clinical reports are unavailable for the NUH dataset; hence, the NUH dataset is only deployed for the segment- and channel-level annotation.

Similarly, the LTMGH dataset consists of routine scalp EEGs. However, unlike the other datasets, the LTMGH EEGs were recorded by EEG recording equipment supplied by a local manufacturer, and not by EEG machines manufactured internationally. Moreover, the LTMGH EEGs were recorded in a warm environment without air conditioning, which induces excessive delta power due to sweat artifacts (see Figure 7). Consequently, the dataset could be prone to more artifacts, potentially increasing the challenges to reliably detect abnormalities in the LTMGH EEGs. As a result, we cannot train the EEG classifiers with this dataset unless we are calibrating the system with this dataset. Moreover, we did not

include segments from this dataset for the segment- and channel-level annotation to avoid confusion for the expert due to the abnormally high delta power.

We apply the following EEG preprocessing steps: a Butterworth notch filter (4th order) at 50Hz (Singapore and India) and 60Hz (USA), a 1Hz high-pass filter (4th order), and the Common Average Referential (CAR) montage. Next, we downsampled all the EEGs to 128Hz. Further, we applied artifact rejection based on noise statistics to remove high amplitude noise.²⁹ This is achieved by computing the mean and standard deviation (std) of the root mean square (rms) amplitude of the EEG signal, then rejecting any 1s epoch (no overlap) with rms amplitude greater than mean + 3 × std.

2.2. EEG frequency features

We investigate the following EEG frequency bands: delta [1,4]Hz, theta [4,8]Hz, alpha [8,13]Hz, and beta [13,30]Hz. The relative power (RP) of each frequency band is calculated as:

$$RP_i = \frac{P_i}{P_{\text{Total}}}, \quad (1)$$

where P_i is the power in frequency band i , $P_{\text{Total}} = \sum P_i$, and $i \in [\delta, \theta, \alpha, \beta]$.

The RP is a normalized index as $RP_\delta + RP_\theta + RP_\alpha + RP_\beta = 1$, and $RP_i \in [0,1]$. From the RP, we derive the power ratios (PR): Primary Ratio Index (PRI), Delta-Alpha-Ratio (DAR), Theta-Alpha-

Table 2. Patient information for the different EEG datasets.

Dataset (F_s)	Total EEG	Slow-free EEG					Slowing EEG				
		EEG	Gender	No	Duration (minutes)	Age (years)	EEG	Gender	No	Duration (minutes)	Age (years)
TUH (250, 256, 500 Hz)	141	99	M	46	22.19±4.36	42.02±14.44	42	M	28	11.58±6.07	52.96±10.39
			F	53	21.26±2.03	46.17±16.87		F	14	19.74±4.09	47.5±18.62
NNI (200 Hz)	114	58	M	29	27.78±0.64	45.62±17.27	56	M	25	27.64±1.58	51.16±18.35
			F	29	27.43±1.95	52.31±19.87		F	31	28.04±1.29	52.94±19.73
Fortis (500 Hz)	358	285	M	155	20.87±6.53	45.86±19.69	73	M	50	20.3±2.95	55.52±17.83
			F	123	20.26±4.07	45.74±18.23		F	19	20.61±3.54	50.0±16.92
			UNK	7	20.68±1.03	43.0±17.86		UNK	4	22.16±1.52	63.75±5.26
LTMGH (256 Hz)	1100	701	M	370	14.01±1.49	33.49±18.29	399	M	207	14.77±1.88	37.03±24.26
			F	331	14.27±1.73	31.04±18.7		F	192	14.65±2.61	36.8±21.79
All	1713	1143	M	600	17.08±5.56	37.93±19.22	570	M	310	16.41±4.88	42.59±23.33
			F	536	17.05±4.58	37.06±20.06		F	256	16.99±5.24	40.32±21.95
			UNK	7	20.68±1.03	43.0±17.86		UNK	4	22.16±1.52	63.75±5.26

Dataset (F_s)	Total EEG	All EEG				
		EEG	Gender	No	Duration (minutes)	Age (year)
NUH (250 Hz)	150	150	M	89	19.36±9.36	51.23±19.91
			F	61	19.60±9.30	56.48±20.18

F_s : sampling frequency, M: male, F: female, UNK: unknown, age/duration are reported as mean \pm std.
Note: The NUH dataset does not have slowing labeled in the clinical report.

Ratio (TAR), and Theta-Beta-Alpha-Ratio (TBAR) (see Table 3). In this paper we consider the following eight spectral features: RP_δ , RP_θ , RP_α , RP_β , PRI, DAR, TAR, and TBAR.

Table 3. Power ratios considered in the study.

Power Ratio	Definition
PRI	$(RP_\delta + RP_\theta)/(RP_\alpha + RP_\beta)$
DAR	RP_δ/RP_α
TAR	RP_θ/RP_α
TBAR	$RP_\theta/(RP_\beta + RP_\alpha)$

2.3. Segment- and channel-level slowing annotation

The supervised learning systems (SSLS and SDLS) require labeled channel-level data to train their channel-level slowing detectors. Therefore, we acquire segments with channel- and segment-level annotations from the TUH, NNI, Fortis, and NUH datasets. The LTMGH dataset is omitted as those EEGs have an abnormal spectrum. We prepared 1000 5s EEG segments consisting of 900 unique segments and 100 duplicate segments (50 unique) for an expert to annotate on the channel- and segment-level.

We select 5s as the segment duration as the minimum cutoff frequency of a slow wave is 1Hz, which corresponds to a period of 1s. Hence, a 5s segment may contain up to five periods of slowing waveforms in any channel, sufficient for slowing detection. We choose the segments according to their PRI values, as

PRI appears to be the most consistent according to our findings. The annotations are performed by one expert in the NeuroBrowser (NB) software.³⁰ The number of slowing and slow-free segments and channels annotated from each dataset are displayed in Table 4. For the segment annotations, the segments are annotated as slow-free and slowing.

Table 4. Summary of annotated slowing segments and channels.

Segment Annotation		
Dataset	Slow-free	Slowing
TUH	154	46
NNI	144	96
Fortis	171	53
NUH	98	135
All	567	330

Channel Annotation			
Dataset	Slow-free	Slowing	Ambiguous
TUH	2926	284	590
NNI	2736	1497	327
Fortis	3249	811	196
NUH	1862	1960	605
All	10773	4552	1718

For channel annotations, all channels from slow-free segments are slow-free. On the other hand, slowing channels from slowing segments are labeled as slowing. The channels that are annotated as slow-free in slowing EEG segments are treated separately as ‘ambiguous’. Slow-free channels in slowing segments are deemed ambiguous as they cannot be treated as

2.4. Proposed EEG classification systems

This section outlines the three proposed EEG classification systems: unsupervised learning system (ULS), supervised shallow learning system (SSLS), and supervised deep learning system (SDLS). We evaluate the systems on three classification problems: channel-, segment-, and EEG-level slowing detection. The systems pipelines are summarized in Table 1. The ULS for the segment- and EEG-level classification is illustrated in Figure 2, while the SSLS and SDLS for the channel-, segment-, and EEG-level classification are illustrated in Figure 3. The classification systems are named after the channel-level detector; the SSLS and SDLS rely on shallow and deep channel-level classifiers, respectively, trained in a supervised manner, whereas in the ULS, the analysis on the channel-level relies on unsupervised learning.

Additionally, all three systems deploy a shallow learning model to perform segment- and EEG-level prediction. We applied five different shallow learning classifiers in this study: Logistic Regression (LR)³¹, SVM (linear and Gaussian/rbf kernel)³², Gradient Boosting (GB)³³, AdaBoost³⁴, and Random Forest (RF)³⁵. The parameters of the shallow learning models are summarized in Table 5. We apply three feature processing steps to the training data to enable efficient training. First, we apply a threshold to the standard deviation (std) to remove non-significant features ($\text{std} \leq 10^{-7}$). Then, we standardize the features by subtracting the mean and dividing by the std. Lastly, we apply Synthetic Minority Over-sampling Technique (SMOTE) with five nearest neighbors to construct synthetic samples of the minority class to match the majority class for training.³⁶ By applying SMOTE to re-balance any imbalanced dataset, we reduce classification bias and improve classification accuracy.

Table 5. Parameters of the shallow learning models.

Shallow Learning Model	Parameter	Value
Logistic Regression	Solver	lbfgs
	Max iteration	10000000
SVM	Kernel	{linear, rbf}
	C	1
	gamma	scale
Gradient Boosting	Estimators	100
	Max features	1
AdaBoost	Estimators	100
Random Forest	Max depth	4
	Estimators	100
	Max features	1

2.4.1. Channel-level classification

Here we describe the single-channel segment (channel-level) slowing detection in the ULS, SSLS, and SDLS. In the ULS, we apply simple thresholding on the eight spectral features computed at single-channel segments. If the spectral feature is above (for RP_δ , RP_θ , PRI, DAR, TAR, and TBAR) or below (for RP_α and RP_β) the threshold, the waveform at that channel exhibits slowing. For the SSLS, we train a shallow learning model on the eight spectral features to detect EEG slowing at the channel-level. Finally, for the SDLS, we train a CNN, whose input is the spectrum of the EEG waveforms.

The EEG spectrum is obtained by transforming 5s EEG signal (640 samples) to the frequency domain [0,64]Hz (321 samples). We discard the frequencies in the [30,64]Hz band to eliminate the gamma band component, keeping only the [0,30]Hz band (150 samples). Finally, we smoothen the spectrum with a moving average (length five). The input of the CNN is the smoothed spectrum (150 samples). We implemented the CNN in Keras 2.2.0³⁷ on an Nvidia GeForce GTX 1080 Graphical Processing Unit (GPU) with Ubuntu 16.04 as the operating system.

We devise the CNN detector (see Figure 4) comparable to the 1D CNN architecture proposed by Thomas et al.¹⁹ First, the convolutional operation is performed by convolving the smoothened EEG spectrum with optimized 1D convolution filters. Next, the resulting convolution outputs are passed through non-linear activation functions. Specifically, we chose Rectified Linear Units (ReLU) as the activation functions. The outputs of these activation functions together form spectral feature maps. The dimensions of the feature maps are reduced by max-pooling. Next, the features are flattened and fed into a fully connected layer. The fully connected layer outputs are mapped into [0,1] with a softmax function, where 0 and 1 correspond to a slow-free and slowing EEG signal, respectively.

We organized the training samples in mini-batches whose size is equal to half the number of slowing waveforms in the training set. To prevent overfitting, we applied balanced training by generating mini-batches with the same number of randomly selected slow waveforms and normal (background) waveforms. Additionally, a dropout of 0.5 is applied

in the fully connected layer. This is set to improve the training efficiency and not to overload the GPU.

The hyperparameters of the CNN are optimized by applying a nested CV on the training data: 80% of the training data is utilized for learning the classifier parameters, the rest is used for validation, i.e., for selecting the CNN hyperparameters and for deciding when to stop the training process.²⁹ The CNN training is halted when the validation cost reaches its minimum. Table 6 lists the settings of the hyperparameters evaluated in our tests. We chose cross-entropy as the objective function of the CNN, and we optimized it by the Adam algorithm.³⁸

Table 6. Optimized hyperparameters in the CNN.

Parameters	Values/Type
Number of convolution layers	1, 2, 3
Number of fully connected layers	1, 2, 3
Number of convolution filters	8, 16, 32, 64, 128
Dimension of convolution filters (kernel)	$1 \times 3, 1 \times 5, 1 \times 7, 1 \times 9, 1 \times 11, 1 \times 13$
Number of hidden neurons	100
Activation functions	ReLU
Dropout probability	0.5
Size of the batch processing	$\frac{n_s}{2}$
Maximum number of iterations	10000
Optimizer	Adam
Learning rate	$10E-4$
Measure	Cross-entropy

n_s : Total number of annotated waveforms.

2.4.2. Segment- and EEG-level classification

All three systems detect slowing at the segment-level and EEG-level by exploiting statistics computed from the individual channels.

When we try to detect slowing in a 5s 19-channel EEG segment, we extract statistics from the 19 channels, and then arrange those 19 values into a histogram. For the ULS and SSSL/SDLS, the statistics are a selected spectral feature, and output of the channel-level slowing detector, respectively. Similarly, when detecting slowing in a full EEG, we first split the full EEG into n 5s segments with a 75% overlap. Next, we extract statistics from all those segments, and arrange those $19n$ values into a histogram. Also, in this case, the statistics are a selected spectral feature and output of the channel-level slowing detector for the ULS and SSSL/SDLS, respectively. We tested several values for the number of bins: 2, 5, 10, 15, or 20 bins. We have reported the selected number of bins in Table 8 and 9, leading to the highest BAC.

For the ULS, we select one of the eight spectral features ($RP_\delta, RP_\theta, RP_\alpha, RP_\beta, PRI, DAR, TAR,$ and $TBAR$) to form the histogram. As different spectral features have different ranges of values for slowing and slow-free EEGs, we must normalize those features extracted across all the single-channel segments. To do so, for each dataset, we randomly select 50 slow-free EEG and compute the histogram of the selected spectral feature, and find the value at $\text{mean} + 3 \times \text{std}$. We perform min-max normalization by dividing that value to all features extracted from the single-channel segments, to ensure that most of the values in slow-free EEGs are bounded between approximately $[0,1]$.

To include the slowing portions exceeding the range of $[0,1]$ (PR for slowing EEG is always greater than in slow-free EEG), we increase the range to $[0,4]$ (see Figure 5). Additionally, we include two additional bins at $[-100,0)$ and $(4, 100]$ to include the outliers but not significantly skew the histogram distribution.

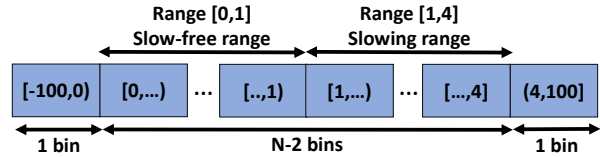


Figure 5. Histogram of ULS.

On the other hand, for the SSSL and SDLS, the selected feature is the output of the single-channel slowing detector (bounded to $[0,1]$). We apply the single-channel slowing detector on all the channels in the 5s EEG segments, and arrange the outputs into a histogram.

With the histograms from the three systems, we extract the histogram-based features: the histogram counts, the mean, median, mode, std, minimum value, maximum value, range, kurtosis, and skewness of the histogram. All three systems deploy a shallow learning model that takes the histogram-based features as input to perform a segment- or EEG-level prediction.

To understand why the histogram-based features are suitable for classification, we display the histograms of PRI for slowing and slow-free EEGs in Figure 6. While slow-free EEGs have a lower average PRI, they still contain a small percentage of single-channel segments with high PRI values. As high PRI values are associated with slowing, this suggests that

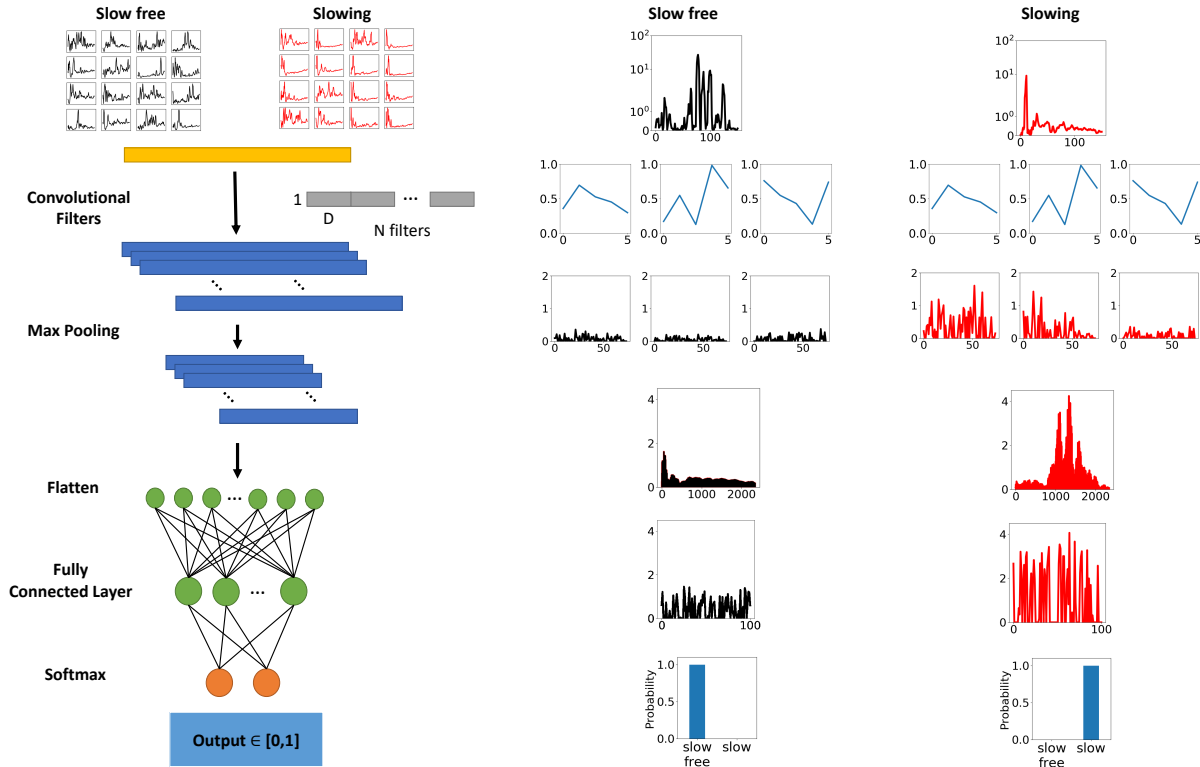


Figure 4. 1D CNN architecture adopted in the study (left), and the activations inside the CNN for a slow-free (middle) and slowing EEG segment (right).

even slow-free EEGs can contain some amount of abnormal slowing, but less frequently than a slowing EEG. Consequently, the histograms-based features can account for the slowing frequency distribution in EEG segments and full EEGs, and can, therefore, serve as useful input features for machine learning methods for detecting slowing in EEG.

2.5. Datasets for training and testing

As mentioned before, we conduct both LOIO and LOSO CV for evaluating the proposed slowing detection systems. In Table 7, we list the various datasets involved in the training and testing of the detection systems in LOIO and LOSO CV. The NUH dataset is always included for training the channel-level slowing detector for EEG-level LOIO CV, as we do not perform EEG-level classification on full EEGs from the NUH dataset. This is because we do not have the slowing labels for the full EEGs for the NUH dataset. The LTMGH dataset is always excluded in the training processes during EEG-level LOIO CV. It is only deployed when evaluating the LTMGH dataset itself with LOSO CV. As we do not have annotated

channels from the LTMGH dataset due to their unusual spectrum, we cannot perform an EEG-level LOSO CV on the LTMGH dataset with the SSLS and SDLS. Instead, we perform a modified LOSO CV, where we train the channel-wise detector with channel data from other datasets as a substitute.

3. Results

3.1. EEG relative power

We compare the relative power (RP) of EEGs of the datasets in Figure 7. The NUH dataset is not included due to the lack of slowing labels. Slowing EEGs have a higher delta and theta RP, with a lower alpha and beta RP than slow-free EEGs. The RP values in the EEGs from the LTMGH dataset are significantly different from those from the TUH, NNI, and Fortis datasets. The EEGs from LTMGH have higher delta RP and a much smaller beta RP. Therefore, it is more meaningful to analyze the LTMGH dataset separately.

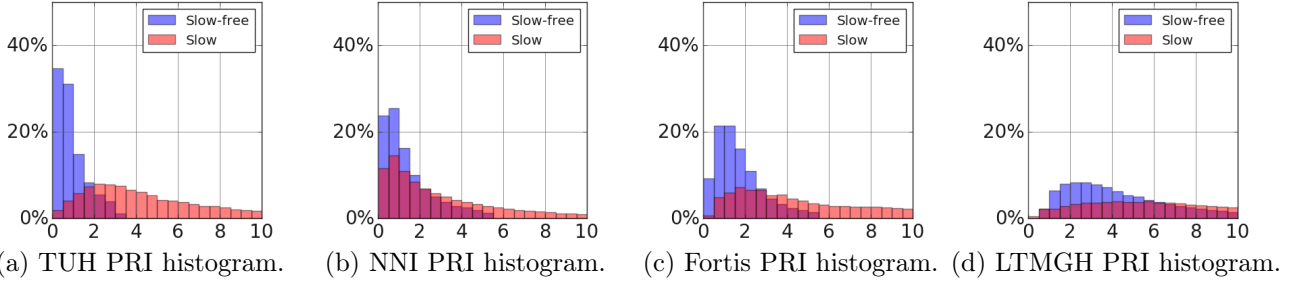


Figure 6. Histograms of PRI values computed from 5s EEG segments. a) TUH, b) NNI, c) Fortis, d) LTMGH. Slowing EEGs have a higher mean and wider distribution of PRI than slow-free EEGs. Additionally, slow-free EEGs can contain high PRI segments, but less frequently. For LTMGH EEGs, the PRI distribution is less distinct, where even slow-free EEGs can contain a substantial number of high PRI segments.

Table 7. Datasets allocation during training and testing for LOIO and LOSO CV.

Testing set	Training set					
	Channel/Segment-level		EEG-level			
	LOIO	LOSO	LOIO		LOSO	
			Channel-level	EEG-level	Channel-level	EEG-level
TUH	NNI, Fortis, NUH	TUH	NNI, Fortis, NUH	NNI, Fortis	TUH	TUH
NNI	TUH, Fortis, NUH	NNI	TUH, Fortis, NUH	TUH, Fortis	NNI	NNI
Fortis	TUH, NNI, NUH	Fortis	TUH, NNI, NUH	TUH, NNI	Fortis	Fortis
NUH	TUH, NNI, Fortis	NUH	-	-	-	-
LTMGH	-	-	TUH, NNI, Fortis, NUH	TUH, NNI, Fortis	TUH, NNI, Fortis, NUH	LTMGH

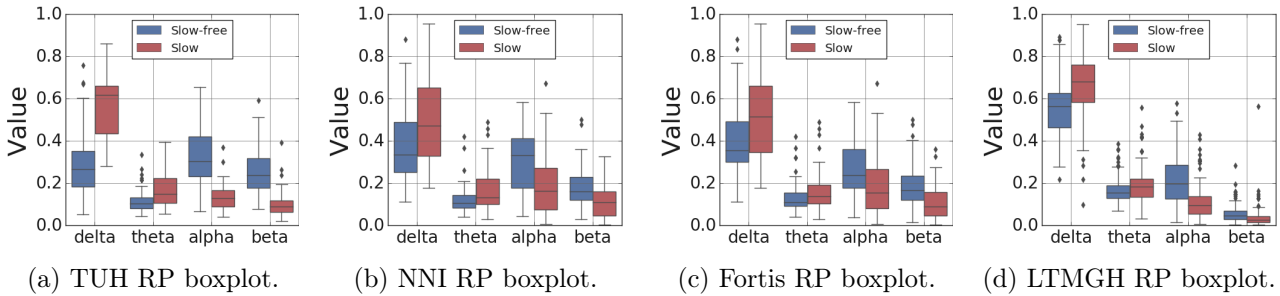


Figure 7. Relative power in the delta, theta, alpha, and beta band: a) TUH, b) NNI, c) Fortis, d) LTMGH. The delta and theta power is stronger in EEGs that exhibit slowing compared to slow-free EEGs. The delta power in LTMGH EEGs is significantly higher than in EEGs from the other datasets.

3.2. Intra-rater agreement (IRA)

In this section, we address the label intra-rater agreement (IRA) of the expert. In this case, the IRA is the percentage of agreement of the labels between the duplicated segments. Theoretically, the slowing detector from the SSLS and SDLS cannot outperform the IRA of the expert, for they are trained with the annotations from the expert. The IRA gives us an approximate upper-limit on the accuracy of our proposed systems.

The channel- and segment-level IRA is 72.4% and 82%, respectively. The disagreements are mainly due to artifacts, eye blinks, or interictal epileptiform

discharges (IEDs), matching observation with the literature.³⁹ In addition, a study performed by Piccinelli et al. reported an IRA of 88.6% for expert agreement for classifying EEGs into three classes: EEGs with IEDs, EEGs with slow waves, and normal EEGs.⁴⁰ Another study on the IRA of IEDs in EEG reported that the median IRA between 9 experts is 80%, comparable to our current observation.⁴¹

3.3. Classification results

The best results for the channel-, segment-, and EEG-level LOIO and LOSO CV for each system, together with their parameters, are displayed in

Table 8 and 9. We list the following performance measures: area under the receiver operating characteristic curve (AUC), area under the precision-recall curve (AUPRC), accuracy (ACC), balanced accuracy (BAC), sensitivity (SEN), and specificity (SPE). Since the number of slowing and slow-free cases is sometimes imbalanced for all three classification tasks, we evaluate the results mainly in terms of BAC.

3.3.1. Channel-level classification results

For LOIO CV, the SSLS and SDLS yield the best performance, both achieving a mean BAC of 71.9%. The ULS obtains a mean BAC of 68.4%. For LOSO CV, the SDLS system yields an impressive mean BAC of 72.4%, besting both the ULS and SSLS. The SDLS performed the best for both cases.

The ULS that deploys thresholding on the PRI achieved the best LOIO and LOSO CV mean BAC, suggesting that PRI is the optimal feature for channel-level slowing identification. All three systems did not perform well on the Fortis dataset, while achieving the best mean BAC on the NNI dataset. The LOIO and LOSO CV results from the three systems achieved comparable channel-level classification accuracy to the channel-level IRA of the expert of 72.4%.

To understand what is learned in the CNN slowing detector in the SDLS, we analyze the feature maps of the convolutional layer in the CNN, as shown in Figure 4. The feature maps revealed that the convolution layer assigns weights in a seemingly random manner to different frequencies in the spectrum (see Figure 8). These optimized quasi-random 1D convolution filters are similar to purely random convolution filters, which were commonly applied in the past to avoid learning the CNN filters, and have been shown to perform well even with limited data.^{42,43}

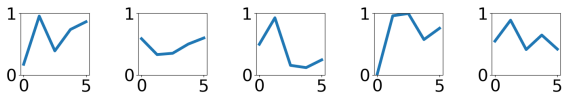


Figure 8. Sample filters with filter length of 5 deployed by the CNN. The filters are optimized by the CNN, but can appear random.

As a verification, we mapped the second fully connected layer of the CNN into a 2D plane through t-Distributed Stochastic Neighbour Embedding (t-SNE) (see Figure 9).⁴⁴ We can observe separable

clusters, indicating that the neurons in the fully connected layers are learning meaningful representation of the EEG waveforms.

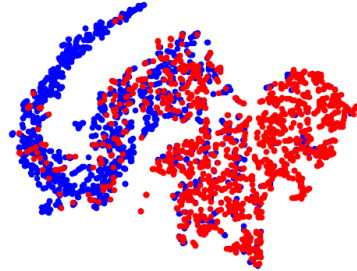


Figure 9. Two-dimensional embedding of the 100-dimensional second fully connected layer in the CNN obtained by t-SNE. The slow-free and slowing EEG segments are marked in blue and red respectively.

3.3.2. Segment-level classification results

For LOIO CV, the SDLS achieves the best mean BAC, followed by the SSLS and the ULS. On the other hand, for the LOSO CV, the SDLS yields the best system performance, followed by the ULS and the SSLS. The SDLS yields the best performance for both LOIO and LOSO CV, achieving a mean BAC of 75.5% and 76.6%, respectively. This BAC is close to the segment IRA of the expert of 82%. Similarly, employing PRI to construct the histograms yielded the best LOIO and LOSO CV results for the ULS. All three systems performed the worst on the Fortis dataset while achieving the best BAC on the NNI dataset.

3.3.3. EEG-level classification results

For LOSO CV, we present the results for classification both with and without the LTMGH dataset. We applied LOSO CV on the LTMGH EEGs, to verify whether the proposed systems perform well on those EEGs after recalibration of the EEG-level classifiers. Since the LTMGH EEGs have unusual spectra, we also report the average results for LOSO CV, excluding those EEGs. For the same reason, we also exclude those EEGs from the LOIO CV analysis.

For LOIO CV (excluding LTMGH dataset), the SDLS achieved the highest mean BAC of 82.0%, with the ULS and SSLS reaching a mean BAC of 80.6% and 79.7%, respectively. However, if we include the LTMGH dataset, the ULS obtains the best mean BAC of 75.7%, which is substantially lower, as the system performed poorly on the LTMGH dataset. All three systems lead to unsatisfactory classification re-

sults for LOIO CV on the LTMGH dataset, as the LTMGH EEGs do not match well with the EEGs from other datasets. Therefore, for EEGs with unusual characteristics (e.g., enhanced delta power as in the LTMGH EEGs), we must recalibrate the EEG-level classification systems. To assess the improvement after recalibration, we perform LOSO CV on all datasets, including LTMGH EEGs.

For LOSO CV (including LTMGH dataset), the ULS achieved the best mean BAC of 80.5%, with a decent classification BAC of 75.8% on the LTMGH dataset. Meanwhile, the SSLs and SDLS achieved a mean BAC below 80.0%, with BAC of around 70.0% on the LTMGH dataset.

One of the reasons that the SSLs and SDLS yield poor results for the LTMGH EEGs may be because we performed a modified LOSO CV on the LTMGH dataset (we do not have labeled channel data from LTMGH to train the channel-level classifier). Hence, the SSLs and SDLS may not be able to detect channel-wise slowing accurately. Instead, deploying a classification system without a channel-level detector such as the ULS to perform EEG-level classification may resolve this issue.

When we exclude the LTMGH dataset, all three systems yield an approximately identical LOSO CV mean BAC of 82.0%. This observation implies that the three systems can generate the same EEG-level classification accuracy after recalibration with EEGs from a particular dataset, despite the different system pipelines. However, this only applies to EEGs recorded under standard conditions (EEGs from TUH, NNI, and Fortis).

If we do not have access to EEG reports to recalibrate the EEG classifiers, the LOIO CV results suggest that the systems could evaluate the EEGs as reliably as a recalibrated system. Omitting the LTMGH dataset, the three systems achieved an LOIO CV mean BAC close to the LOSO CV mean BAC of 82.0% achieved by all three systems.

The SDLS achieves an almost identical mean BAC of approximately 82.0% for both LOIO and LOSO CV (excluding the LTMGH dataset). This implies that the SDLS can potentially perform equally well in both scenarios. Moreover, this is the best BAC that we have obtained for the given current datasets and clinical reports.

In summary, we have demonstrated the need to evaluate the systems via both LOIO and LOSO CV.

The LOSO CV BAC values are usually better than the ones in LOIO CV, since the EEG classifiers are trained and tested on EEGs of the same institutions. Therefore, the classifiers are effectively recalibrated to the EEGs of that institution. Hence, if EEG data is available, it is advisable to retrain the EEG classifiers on EEG data (and corresponding reports) from the institution where it will be deployed.

If such data is unavailable, our LOIO CV results suggest that reliable detection of EEG slowing can still be achieved through EEG classifiers trained on EEGs from other institutions. For EEG recorded under unusual circumstances that do not generalize well, retraining of the EEG classifiers might be required; we have shown for the LTMGH EEGs that reliable slowing detection can be obtained after recalibration.

3.4. *Threshold-based EEG-level classification*

In this section, we show how shallow learning models can accurately detect EEG slowing through histogram-based features. The ULS deploys spectral features (the PRI is selected for illustration, as it yields the best results), while the SSLs and SDLS rely on histograms of the outputs of the channel-level slowing detector. We plot the average histogram distribution (20 bins) of all EEGs across the datasets (TUH, NNI, Fortis) in Figure 10. The histograms are split based on the EEG-level LOIO CV classification results of the respective systems: true positive (TN), true negative (TN), false positive (FP), and false negative (FN).

The histograms show differences across slow-free and slowing EEGs for the three systems. The ULS detects pathological slowing in an EEG if it detects a high percentage of single-channel segments with high PRI values. On the other hand, the SSLs and SDLS detect abnormal slowing in an EEG when the output of the single-channel slowing detector is frequently close to 1. The histogram from the SDLS is more skewed than those in the SSLs. To compare the slowing and slow-free EEGs, we define a normal EEG background segment to be between bin 1 to 5, and a slow EEG segment to be between bin 15 to 20. The bins between 6 and 14 are not included. The PRI values and slowing detector outputs corresponding to the bin numbers are listed in Table 10. In Figure 11,

Table 8. Channel-, segment- and EEG-level LOIO CV results for the different datasets.

Classification	System	Dataset	Parameters	Results					
				AUC	AUPRC	ACC	BAC	SEN	SPE
Channel	ULS	TUH	CC: Threshold PRI	0.830	0.415	0.708	0.744	0.785	0.702
		NNI		0.819	0.698	0.748	0.733	0.686	0.779
		Fortis		0.633	0.250	0.652	0.585	0.477	0.693
		NUH		0.749	0.677	0.665	0.676	0.779	0.574
		Mean		0.758	0.510	0.693	0.684	0.682	0.687
	SSLS	TUH	CC: LR	0.862	0.575	0.752	0.772	0.796	0.747
		NNI		0.857	0.773	0.782	0.762	0.694	0.831
		Fortis		0.689	0.309	0.677	0.632	0.556	0.708
		NUH		0.786	0.782	0.712	0.709	0.821	0.597
		Mean		0.798	0.610	0.731	0.719	0.717	0.721
	SDLS	TUH	CC: CNN (F:64, K:13)	0.827	0.349	0.655	0.723	0.806	0.640
		NNI		0.847	0.732	0.768	0.768	0.769	0.767
		Fortis		0.743	0.395	0.663	0.668	0.677	0.660
		NUH		0.791	0.762	0.720	0.717	0.845	0.588
		Mean		0.802	0.560	0.701	0.719	0.774	0.664
	Segment	ULS	TUH	Feature: PRI SC: LR Bins: 5	0.761	0.517	0.732	0.678	0.581
NNI			0.884		0.852	0.818	0.807	0.755	0.859
Fortis			0.649		0.376	0.654	0.590	0.446	0.734
NUH			0.758		0.818	0.691	0.677	0.782	0.573
Mean			0.763		0.641	0.724	0.688	0.641	0.735
SSLS		TUH	CC: LR SC: LR Bins: 2	0.812	0.598	0.784	0.753	0.698	0.808
		NNI		0.896	0.868	0.831	0.821	0.777	0.866
		Fortis		0.694	0.428	0.692	0.664	0.6	0.728
		NUH		0.77	0.81	0.699	0.69	0.759	0.621
		Mean		0.793	0.676	0.751	0.732	0.708	0.756
SDLS		TUH	CC: CNN (F:64, K:13) SC: LR Bins: 10	0.767	0.466	0.745	0.758	0.783	0.734
		NNI		0.842	0.771	0.817	0.811	0.781	0.84
		Fortis		0.765	0.547	0.754	0.742	0.717	0.766
		NUH		0.783	0.785	0.725	0.708	0.815	0.602
		Mean		0.789	0.642	0.76	0.755	0.774	0.736
EEG		ULS	TUH	Feature: PRI SC: GB Bins: 20	0.95	0.926	0.923	0.897	0.96
	NNI		0.71		0.786	0.728	0.724	0.948	0.5
	Fortis		0.847		0.677	0.863	0.796	0.909	0.682
	LTMGH		0.714		0.637	0.698	0.611	0.963	0.26
	Mean		0.805		0.757	0.803	0.757	0.945	0.569
	Mean*		0.836		0.796	0.838	0.806	0.939	0.672
	SSLS	TUH	CC: SVM SC: LR Bins: 2	0.946	0.895	0.923	0.911	0.881	0.941
		NNI		0.754	0.763	0.702	0.700	0.607	0.793
		Fortis		0.838	0.664	0.790	0.781	0.765	0.797
		LTMGH		0.713	0.570	0.423	0.539	0.964	0.114
		Mean		0.813	0.723	0.710	0.733	0.804	0.661
	Mean*	0.846	0.774	0.805	0.797	0.751	0.844		
	SDLS	TUH	CC: CNN (F:64, K:9) SC: LR Bins: 10	0.961	0.919	0.901	0.916	0.952	0.879
		NNI		0.728	0.778	0.728	0.726	0.589	0.862
		Fortis		0.847	0.674	0.855	0.817	0.753	0.882
		LTMGH		0.598	0.390	0.376	0.506	0.982	0.030
Mean		0.783		0.690	0.715	0.741	0.819	0.663	
Mean*		0.845		0.790	0.828	0.820	0.765	0.874	

CC: Channel classifier, SC: Segment/EEG classifier, Bins: Histogram bins.

ACC: Accuracy, BAC: Balanced Accuracy, SEN: Sensitivity, SPE: Specificity, F: Number of filters, K: Filter size.

*: Excluding the LTMGH dataset.

Table 9. Channel, segment, and EEG-level LOSO CV results for the different datasets.

Classification	System	Dataset	Parameters	Results					
				AUC	AUPRC	ACC	BAC	SEN	SPE
Channel	ULS	TUH	CC: Threshold PRI	0.830	0.415	0.837	0.763	0.676	0.850
		NNI		0.819	0.698	0.736	0.738	0.745	0.731
		Fortis		0.633	0.250	0.545	0.614	0.726	0.502
		NUH		0.749	0.677	0.690	0.685	0.648	0.723
		Mean		0.758	0.510	0.702	0.700	0.699	0.702
	SSLs	TUH	CC: SVM_rbf	0.676	0.174	0.826	0.677	0.496	0.858
		NNI		0.828	0.695	0.773	0.776	0.788	0.764
		Fortis		0.626	0.308	0.648	0.602	0.525	0.679
		NUH		0.759	0.737	0.707	0.707	0.677	0.738
		Mean		0.722	0.479	0.739	0.691	0.622	0.760
	SDLS	TUH	CC: CNN (F:32, K:7)	0.791	0.237	0.715	0.762	0.820	0.704
		NNI		0.837	0.667	0.738	0.765	0.856	0.674
		Fortis		0.725	0.390	0.621	0.655	0.713	0.598
		NUH		0.804	0.812	0.718	0.715	0.824	0.606
		Mean		0.789	0.527	0.698	0.724	0.803	0.646
	Segment	ULS	TUH	Feature: PRI SC: LR Bins: 5	0.827	0.690	0.809	0.769	0.698
NNI			0.858		0.818	0.775	0.758	0.670	0.845
Fortis			0.689		0.539	0.692	0.669	0.615	0.722
NUH			0.692		0.749	0.644	0.658	0.549	0.767
Mean			0.766		0.699	0.730	0.713	0.633	0.794
SSLs		TUH	CC: SVM_rbf SC: RF Bins: 5	0.745	0.491	0.742	0.710	0.651	0.768
		NNI		0.845	0.732	0.822	0.818	0.798	0.838
		Fortis		0.586	0.351	0.650	0.582	0.431	0.734
		NUH		0.703	0.760	0.661	0.671	0.594	0.748
		Mean		0.720	0.584	0.719	0.695	0.619	0.772
SDLS		TUH	CC: CNN (F:32, K:7)	0.749	0.511	0.825	0.780	0.696	0.864
		NNI		0.851	0.772	0.829	0.832	0.844	0.819
		Fortis		0.747	0.455	0.723	0.715	0.698	0.731
		NUH		0.748	0.745	0.742	0.737	0.770	0.704
		Mean		0.774	0.621	0.780	0.766	0.752	0.780
EEG		ULS	TUH	Feature: 4 RP SC: GB Bins: 20	0.942	0.906	0.923	0.911	0.941
	NNI		0.76		0.775	0.746	0.744	0.828	0.661
	Fortis		0.846		0.706	0.872	0.806	0.918	0.694
	LTMGH		0.829		0.72	0.762	0.758	0.775	0.74
	Mean		0.844		0.777	0.826	0.805	0.866	0.744
	Mean*		0.849		0.796	0.847	0.820	0.896	0.745
	SSLs	TUH	CC: RF SC: LR Bins: 5	0.919	0.897	0.895	0.884	0.857	0.911
		NNI		0.828	0.844	0.772	0.771	0.714	0.828
		Fortis		0.831	0.641	0.863	0.804	0.706	0.903
		LTMGH		0.743	0.609	0.732	0.716	0.657	0.774
		Mean		0.830	0.748	0.815	0.794	0.734	0.854
		Mean*		0.859	0.794	0.843	0.820	0.759	0.881
	SDLS	TUH	CC: CNN (F:32, K:5) SC: LR Bins: 15	0.943	0.853	0.922	0.917	0.905	0.929
		NNI		0.774	0.801	0.754	0.751	0.571	0.931
		Fortis		0.836	0.652	0.841	0.786	0.694	0.879
		LTMGH		0.723	0.573	0.704	0.690	0.639	0.741
		Mean		0.819	0.720	0.805	0.786	0.702	0.870
		Mean*		0.851	0.769	0.839	0.818	0.723	0.913

CC: Channel classifier, SC: Segment/EEG classifier, Bins: Histogram bins.

ACC: Accuracy, BAC: Balanced Accuracy, SEN: Sensitivity, SPE: Specificity, F: Number of filters, K: Filter size.

*: Excluding the LTMGH dataset.

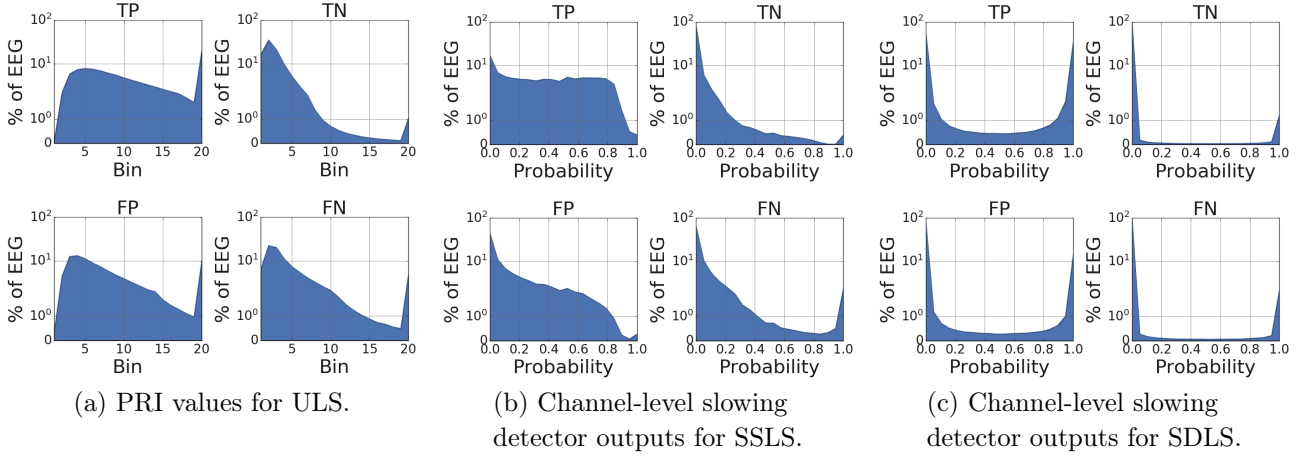


Figure 10. Distribution of PRI values for ULS (a) and of channel-level slowing detector outputs for SSLS (b) and SDLS (c). Distributions for the TP, FN, FP, and FN of the classification results are displayed. The y-axis is in symmetric log scale.

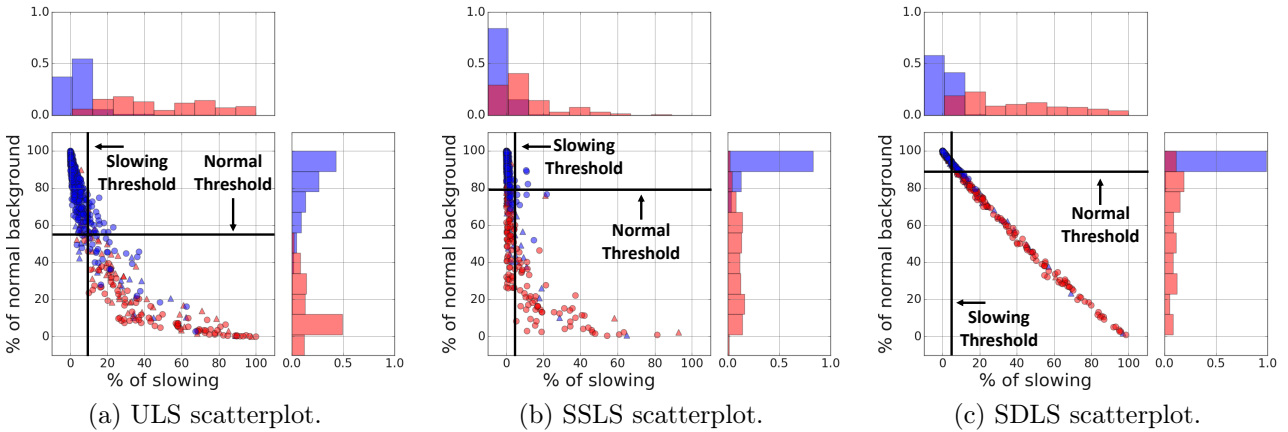


Figure 11. EEG-level slowing versus background percentage scatterplot. a) ULS, b) SSLS, c) SDLS. Slow-free and slowing EEGs are denoted in blue and red, respectively. The normalized histogram distribution of the percentage of normal and slowing segments is illustrated on the top and right sides of each scatterplot. From the scatterplot, we can determine the best threshold.

we display scatterplots of the percentage of normal EEG background versus the percentage of slowing.

Table 10. Histogram bins and their corresponding PRI and slowing detector outputs.

Bin range	ULS	SSLS and SDLS
	PRI range	Slowing detector output range
[1,5]	0-2.822	0-0.25
[6,14]	2.822-9.984	0.25-0.75
[15,20]	9.984	0.75-1

The scatterplot for the ULS and SSLS displayed a non-linear pattern, while for the SDLS, it generated a linear trend. The linearity of the SDLS scatterplot is due to the skewed output distribution of the slowing detector (see Figure 10). The slow-free

and slowing EEG exhibit clear distinctions for the three systems, enabling us to apply thresholding on the percentage of normal background or slowing duration to classify the EEGs. We tested all histogram bins as potential thresholds for the binary classification. For each system, we utilize different threshold to compute the classification BAC for each dataset (TUH, NNI, Fortis), and take the mean BAC. The thresholds associated with the highest mean BAC for each system are listed in Table 11.

As both the SSLS and SDLS leverage the histograms of the channel-level slowing detector outputs, they have similar optimal thresholds. The ULS has the best overall mean BAC of 80.9% with a

55% threshold on the percentage of the normal background. The SSSL and SDLS achieve a mean BAC of 80.0% and 78.0% with a threshold on the normal background percentage set at 80% and 90%, respectively. A threshold on the normal background percentage yields better classification results than a threshold on the slow percentage. Thresholding is more interpretable and can yield comparable results to the EEG-level LOIO and LOSO CV with the shallow learning model.

Table 11. EEG-level classification mean BAC with threshold.

System	Normal Background %		Slowing %	
	Threshold	BAC	Threshold	BAC
ULS	55	0.809	10	0.786
SSLS	80	0.800	5	0.649
SDLS	90	0.780	5	0.777

3.5. Four degrees of slowing in EEG

Four degrees of slowing can be distinguished from the EEG slowing duration (intermittent or persistent) and localization (focal or generalized). With the literature as a guideline^{6,7}, slowing is persistent when it occurs in over 50% of the EEG recording. Otherwise, it is intermittent if it occurs between 11 to 49% of the EEG recording. Any EEG with a slowing duration of under 11% is slow-free. Here, we increase the lower limit to 20% to ensure that we only capture EEGs with abnormal amount of slowing. Likewise, slowing can be considered generalized if it occurs at more than half of the scalp electrodes, and is considered localized otherwise.^{6,7}

We detect the channels that exhibit slowing longer than 20% in the recording to determine the slowing localization. If the number of detected channels is more than 50% of the total number of channels, the EEG contains generalized slowing. Otherwise, it is focal slowing. Next, we compute the average percentage of slowing duration in those detected channels. If the percentage is over 50%, it is considered persistent slowing. Otherwise, it is intermittent slowing.

We illustrate the four degrees of EEG slowing in Figures 12 and 13. The scatterplot is divided into four quadrants at the 50% mark on both axes to reveal four regions: generalized persistent slowing (GPS), generalized intermittent slowing (GIS), focal persistent slowing (FPS), and focal intermittent slowing (FIS). From the SDLS scatterplot, we select an EEG example for each degree of slowing and a

slow-free EEG (case 1 to 5). We plot scalp heatmaps of the percentage of slowing for each case in Figure 13 to differentiate the different degrees of slowing visually from the contours.

4. Discussion

4.1. Comparison of the proposed classification systems

Excluding the LTMGH dataset, the SDLS exhibits the best overall classification performance for the three classification problems for both LOIO and LOSO CV. However, when we include the LTMGH dataset, the ULS yields better EEG-level LOSO CV results. Examining the results from the SSSL and SDLS also show that a channel-level slowing detector based on deep learning is superior to one based on shallow learning. Therefore, it is recommended to deploy the SDLS instead of the SSSL.

The results suggest that we should always recalibrate the systems to bestow superior classification accuracy. Otherwise, we train the proposed systems with EEG data from other institutes. Assuming we have EEGs from a new dataset, we should always deploy the SDLS for most cases as it is superior to the ULS. Even if channel-level annotations are unavailable for this dataset, we can deploy a slowing detector trained on other datasets, and only retrain the EEG classifier on the EEGs from the target center. However, we should deploy the ULS if the EEGs are recorded under non-standard conditions that may result in distortions in the EEG. The SDLS is not suitable in this situation, as the EEGs are not generalizable.

Therefore, we should always recalibrate the systems if possible. Otherwise, we train the proposed systems with EEGs from other institutes. The SDLS is suitable for most situations besides when the EEGs are recorded under unusual conditions. In such cases, we should deploy the ULS.

4.2. Comparison of the EEGs from different datasets

The performance of the three EEG classification systems varies across the different datasets. The classification results for the TUH dataset are consistently excellent, probably because the dataset is prepared explicitly for slowing EEG related research. Therefore, the clinical reports might be more reli-

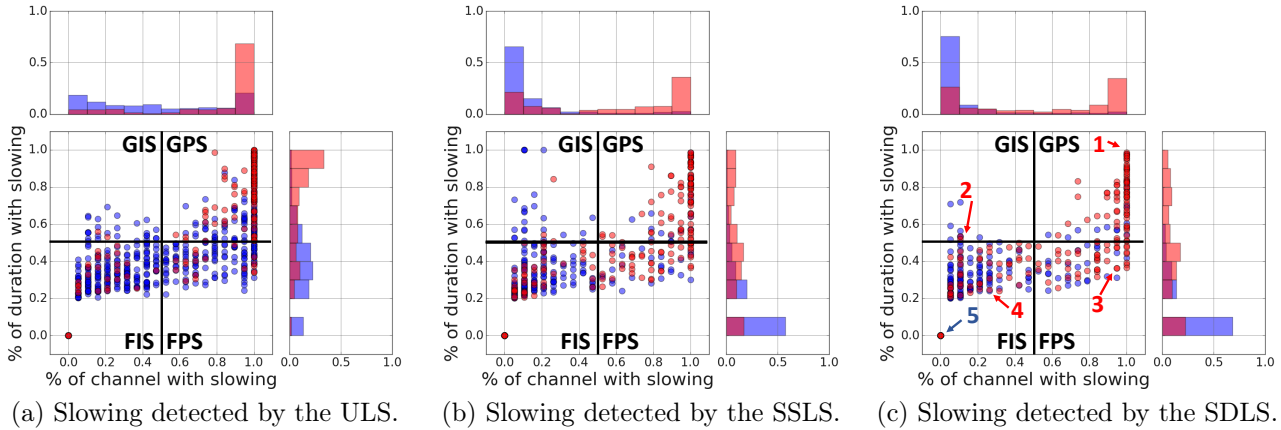


Figure 12. Four degrees of slowing (GPS, GIS, FPS, and FIS) were detected in EEG-level for the a) ULS, b) SSLs, c) SDLS. Each blue and red dot represents a slow-free EEG and a EEG with pathological slowing, respectively. We display an example of GPS, GIS, FPS, and FIS and a slow-free EEG detected by SDLS in Figure 13.

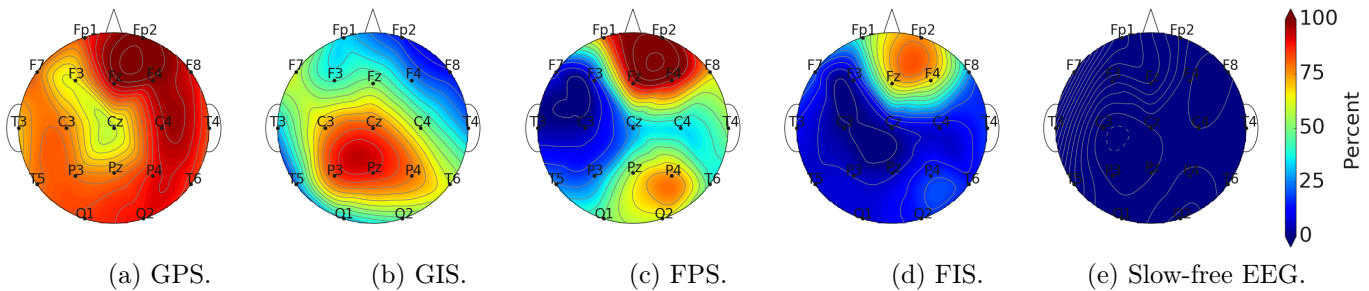


Figure 13. Examples of EEGs with different degrees of slowing and a slow-free EEG. The percentage of slowing for each channel is displayed.

able and accurate. On the other hand, the NNI and Fortis datasets were created without such specifications nor selection biases. Hence, their clinical reports may contain less reliable information regarding slowing, leading to poorer results. However, the NNI and Fortis datasets may be more in line with routine EEGs recorded and interpreted in clinical practice. The three systems perform the worst on the LTMGH dataset, although the data collection method is the same as the NNI and Fortis datasets. This is because the EEGs from LTMGH have unusual EEG spectra, and the distorted spectra may hurt the classification performance, as suggested by the results.

There are also various degrees of slowing across the datasets. From the TUH dataset clinical reports, most EEG slowing appears to be generalized and/or persistent. In contrast, the slowing EEGs in the NNI and Fortis dataset is often focal and/or intermittent. Generalized and persistent slowing implies a more severe neurological condition, which might be easier to detect. Therefore, the TUH dataset is expected to

have more reliable classification results than the NNI and Fortis datasets. The LTMGH dataset did not specify the severity of slowing in the clinical report. However, the slowing detected for LTMGH EEGs are similar to the NNI and Fortis EEGs. Hence, the slowing EEGs from the LTMGH dataset are mostly focal and intermittent, and thus should perform poorer than the TUH dataset.

4.3. Comparison to the literature

As far as we know, automated methods to detect pathological slowing have not yet been proposed in the literature. Instead, existing studies concentrate on detecting neurological disorders that induce slowing. In this context, most papers concern ischaemic stroke (IS), as we will briefly review in the following.^{1,13,16}

Finnigan et al. investigated the DAR to predict the presence of IS. They proposed a threshold of $DAR = 3.7$, which results in specificity and sensitiv-

ity of 100% for detecting IS, corresponding to a 100% classification accuracy.¹⁶ However, they assessed the method on only 46 subjects (28 healthy and 18 with IS), and the data originated from only one center.

Similarly, Sheorajpanday et al. deployed the PRI (named Delta-Theta-Alpha-Beta Ratio (DTABR) their study) to determine the presence and absence of an IS in lacunar circulation stroke (POCS) and posterior circulation stroke (LACS).¹ They reported that the PRI is not significantly different for POCS. On the other hand, they stated that $PRI < 1$ was 100% specific for the absence of recent IS, while $PRI > 3.5$ was 100% sensitive for the presence of an IS in LACS. The optimal accuracy is achieved at $PRI = 1.75$, where the classification sensitivity, specificity, accuracy, and AUC are 73.0%, 67.0%, 71.0%, and 0.78, respectively. However, for predicting the unfavorable outcome of IS, at $PRI = 2.4$, they achieved a sensitivity, specificity, accuracy, and AUC of 100%, 77.0%, 83.0%, and 0.88, respectively. They evaluated their technique on a small dataset of 60 subjects (36 subjects with POCS and 24 subjects with LACS), recorded at the same center.

Similarly, Bentes et al. deployed two quantitative EEG indices to predict whether the post-stroke functional outcome is favorable at discharge and after 12 months.¹³ The alpha RP achieved a CV AUC of 0.814 and 0.852 at discharge and after 12 months, respectively. The PRI (named DTABR in the study) reached a CV AUC of 0.827 and 0.859 at discharge and after 12 months, respectively. They evaluated their methods on EEGs from 151 patients with consecutive anterior circulation ischemic stroke (112 male and 39 female), recorded from the same center.

We cannot directly compare our results with those reported in the three studies^{1,13,16}, as the classification problems are different. Nonetheless, we can estimate how well our proposed system may fare in comparison. We compare the EEG-level LOSO CV results to the literature as the studies investigate EEGs from a single center. Excluding the LTMGH dataset, the SDLS yields an EEG-level LOSO CV mean sensitivity, specificity, accuracy, and BAC of 72.3%, 91.3%, 83.9%, and 81.8%, respectively, with a mean AUC of 0.851 for detecting pathological slowing. The proposed SDLS achieved better results than reported in Sheorajpanday et al. However, they are

inferior to the results of Finnigan et al., while the study of Bentes et al. reported an AUC value on par with our study. Hence, our proposed SDLS achieved comparable results as compared to literature.

However, we evaluated our proposed systems on multiple independent datasets, accounting for 613 subjects (442 and 171 subjects with slowing and no slowing, respectively) from three countries and three institutes (if we omit the LTMGH dataset). Including the LTMGH dataset, we have 1713 subjects (1143 and 570 subjects with slowing and no slowing, respectively) from three countries and four institutes. Furthermore, we assessed our systems for both LOIO and LOSO CV scenarios, while all the studies only tested their method via LOSO CV. More importantly, our systems are not restricted to stroke prediction, as it detects pathological slowing in general. Consequently, they can be applied to identify disorders that induce pathological slowing.

4.4. Computational complexity

We assess the processing time required for classifying a 30-minute routine EEG by the three proposed systems. The experiments were conducted in Python v3.7 with an Intel (R) Core^(TM) i5-6500 CPU @ 3.20G Hz and a Nvidia GeForce GTX 1080 Graphical Processing Unit (GPU) with Ubuntu 16.04 as the operating system. The evaluation was executed over 100 trials, and the statistics are summarized in Table 12.

The SDLS is the most computationally efficient, with a mean processing duration of around 4s, as the system runs the CNN on the GPU. The ULS and SSLs took almost 12 times longer to process the EEG. Most of the time is spent on extracting spectral features for the channel-level slowing detector. Consequently, the SDLS is fast enough for clinical applications and be operated in real-time such as monitoring in the ICU or fast triage in the emergency department, whereas the ULS and SSLs would require more efficient implementations for such purposes.

For instance, we can parallelize the feature extraction method, and extract at each channel in parallel; such parallel scheme would lead to a drastic speed-up. Moreover, we can reduce the overlap percentage to reduce the number of segments as computation time for the channel-level features extraction module is proportional to the number of segments.

Table 12. Processing time required for a 30-minute EEG (128Hz).

System	Pre-processing	Artifact rejection	Channel-level features extraction	Channel-level classification (CPU + GPU)	Histogram features extraction	EEG-level classification	Mean total time required
ULS	1.1±0.12	1.7±0.037	45.3±0.54	-	0.19±0.089	0.09±0.04	48.4
SSLS	1.1±0.12	1.7±0.037	45.3±0.54	0.04±0.13	0.007±0.002	0.27±0.047	48.4
SDLS	1.1±0.12	1.7±0.037	-	1.1±0.28	0.009±0.001	0.16±0.008	4.08

Time is reported as mean \pm std seconds.

However, we will have to determine the optimal overlap percentage to prevent compromising the classification performance.

5. Conclusions and Future work

We proposed three automated systems to detect pathological slowing in EEG. Slowing can be detected on the channel-, segment-, and EEG-level. We evaluated the proposed systems on datasets from TUH, NNI, Fortis, NUH (only channel- and segment-level), and LTMGH (only EEG-level). The SDLS yielded the best overall classification results (excluding LTMGH): LOIO CV mean BAC of 71.9%, 75.5%, and 82.0%, for the channel-, segment- and EEG-level classification, respectively, and LOSO CV mean BAC of 73.6%, 77.2%, and 81.8%, for the channel-, segment-, and EEG-level classification, respectively. The ULS and SSLS approach the EEG-level performance of the SDLS with a BAC of 82% for LOSO CV, but underperform in other situations.

The channel and segment-level performance of the SDLS has an LOIO CV mean BAC of 71.9% and 77.2%, which is similar to the channel and segment IRA of the expert, which stands at 72.4% and 82%, respectively. This suggests that the SDLS system can detect EEG slowing channel- and segment-wise on par with a human expert. Similarly, the EEG-level results for the three systems are comparable to human experts as it lies within the range of the inter-rater agreement of 80% for detecting IED patterns in EEG.⁴¹ At present, there are no similar inter-rater agreement studies for EEG slowing, which would be a more relevant benchmark for automated detection of EEG slowing.

To gain more insights into the automated detection of EEG slowing, we developed and assessed the histogram-based features of the EEGs. By defining the percentage of slowing and normal background, we deployed a threshold-based EEG-level classification method that yields decent accuracy. Moreover, we define the four degrees of slowing based on dura-

tion and spatial extent of EEG slowing and visualize the various EEG slowing on the scalp. The various degrees of slowing can provide helpful information for diagnostic purposes.

The SDLS can evaluate a 30-minute EEG in around 4s, allowing real-time clinical applications such as continuous ICU monitoring or brain surgery. It can eventually be deployed to help neurologists diagnose cerebral dysfunction that induce pathological slowing, such as stroke, epilepsy, or dementia.

This study has several limitations. The proposed systems have only been tested on EEGs recorded while the subjects are awake. In future work, we will train models to handle sleep EEGs. Additionally, while we can detect slowing, specifically the duration and spatial extent of EEG slowing, they were not validated, as we do not have reliable ground truth on the degrees of slowing. Detailed slowing information is often not specified in the clinical report. In the future, we want to collect annotations from more than one expert, to develop the channel-level slowing detector based on the opinions of multiple experts. With more opinions, we can also investigate the slowing inter-rater agreement across disparities across multiple experts. Finally, we plan to increase our pool of datasets to enhance the generalizability of our systems.

Conflicts of Interest

The authors have no disclosures to report.

Acknowledgments

The NUH and NNI datasets were collected under the supervision of Dr. Rahul Rathakrishnan and Dr. Yee-Leng Tan, respectively, supported by the National Health Innovation Centre (NHIC) grant (NHIC-I2D-1608138).

Appendix

A. EEG segment preparation

We prepared 1000 5s EEG segments to be annotated by an expert on both channel- and segment-level. We included waveforms that are likely to be slow-free, in addition to waveforms that most likely exhibit slowing. The PRI is selected as a slowing measure due to its excellent segregation performance for stroke-related conditions.¹ Indeed, it has been reported that the average PRI value across 19 channels yields 100% specificity for $PRI < 1$, and 100% sensitivity for $PRI > 3.5$.

Similarly, we select segments with $PRI \geq 3.5$ to include highly probable slowing segments. We also include a small number of segments with PRI in-between $1 < PRI < 3.5$ to include segments that should contain more slow-free channels. Segments with PRI value $PRI < 1$ are not selected as the majority of the channels are expected to be slow-free. The segment length is 5s to allow the segment to contain up to five periods of slowing waveform in any channel. We extracted waveforms from the TUH, NNI, Fortis, and NUH dataset to obtain annotated segments and channels, and select the waveforms for annotation according to the following procedure:

- (1) We apply the EEG preprocessing methods described in Section II and split the EEG into 5s segments and extract the average PRI values across the 19-channels.
- (2) We remove segments that contain noticeable artifacts by visual inspection.
- (3) We randomly select 950 unique segments, with approximately equal numbers from the TUH, NNI, Fortis, and NUH datasets. We select a maximum of 20 segments from each EEG, in order to include waveforms from a large variety of EEGs. Additionally, we select the segments such that 90% of the segments have $PRI > 3.5$ (probable slowing segment), and 10% of the segments have $1 < PRI < 3.5$ (ambiguous).
- (4) We create copies of 50 randomly selected waveforms (one copy for each of the 50 waveforms), and randomize the order of all the segments.

One expert annotated the segments and channels in NeuroBrowser (NB).³⁰ The expert also pointed out other types of waveforms, including artifacts, ictal activities, spikes, eye blinks, K-complexes,

photic stimulations, or NIL (no comments).

B. PRI values distribution of slowing EEG channels and segments

We removed the 100 duplicate segments from the 1000 segments and analyzed the PRI of the remaining 900 segments and channels in Table 13. The segments are split into two categories, slowing and slow-free, as annotated by the expert. We notice that the PRI values of the Fortis segments have comparable PRI values for slowing and slow-free EEGs, which can lead to challenges during classification. As seen in Table 8 and 9, the channel- and segment-level results for the Fortis dataset are much poorer than those from TUH, NNI, and NUH datasets.

Table 13. Summary of the PRI values extracted from segment annotations.

Dataset	Slow-free Segment PRI			Slowing Segment PRI		
	No	Mean	std	No	Mean	std
TUH	151	5.544	3.366	43	15.647	11.721
NNI	142	5.632	3.571	94	21.798	30.808
Fortis	169	7.36	4.621	65	9.094	4.819
NUH	103	7.409	5.986	133	17.722	13.213
All	565	6.449	4.455	335	16.926	19.341

We divide the channels into three categories: slow-free (channels from segments labeled as ‘slow-free’), slowing (channels labeled as ‘slowing’ from segments labeled as ‘slowing’), and ambiguous (channels labeled as ‘slow-free’ from segments labeled as ‘slowing’).

We summarize the distribution of the channel PRI values in Table 14 according to the three categories. The ambiguous channels are supposed to be free of slowing, but have higher PRI values than slow-free channels, and lower PRI values than slowing channels. We discard the ambiguous channels from our analysis and training process to avoid false positives, as we cannot confidently assume they are slow-free. Again, the PRI values from the Fortis channels between slowing and slow-free are similar.

C. PRI values for events waveform

In Table 15, we show PRI values of the events mentioned by the expert in the comments. The segments containing spikes, eye blinks, and K-complex waveforms have a much higher PRI value on average. By contrast, segments containing artifacts, ictal activity,

Table 14. Summary of the PRI values extracted from channel annotations.

Dataset	Slow-free Channel PRI			Slowing Channel PRI			Ambiguous Channel PRI		
	No	Mean	std	No	Mean	std	No	Mean	std
TUH	2869	5.544	5.185	263	25.192	33.307	554	11.115	11.189
NNI	2698	5.632	7.668	1473	24.615	39.189	313	8.544	7.253
Fortis	3211	7.360	8.492	1053	9.426	8.104	182	7.178	6.900
NUH	1957	7.409	8.510	1940	18.573	18.689	587	14.913	17.218
All	10735	6.449	7.585	4729	18.786	27.025	1636	11.548	13.119

and photic stimulation waveforms have a much lower PRI value. As high PRI value is a feature of slowing, this implies that sharp spike waveforms can generate slow-like features, while waveforms with artifacts can appear slow-free.

Table 15. Summary of the PRI values extracted from events.

Event	Slow-free Segment PRI			Slowing Segment PRI		
	No	Mean	std	No	Mean	std
Artifact	72	6.125	3.678	8	9.751	4.196
Ictal	12	5.323	2.504	10	7.868	3.767
Spike	7	9.691	6.235	3	14.714	10.311
Eye blink	9	12	9.791	2	27.091	25.297
K-complex	5	12.865	15.53	1	34.195	-
Photic	0	-	-	1	3.897	-
NIL	460	6.302	4.072	311	17.335	19.828
All	565	6.449	4.455	335	16.926	19.341

Bibliography

1. R. V. Sheorajpanday, G. Nagels, A. J. Weeren and P. P. De Deyn, Quantitative eeg in ischemic stroke: correlation with infarct volume and functional status in posterior circulation and lacunar syndromes, *Clinical Neurophysiology* **122**(5) (2011) 884–890.
2. A. W. Kaszniak, D. C. Garron, J. H. Fox, D. Bergen and M. Huckman, Cerebral atrophy, eeg slowing, age, education, and cognitive functioning in suspected dementia, *Neurology* **29**(9 Part 1) (1979) 1273–1273.
3. E. M. Donnelly and A. S. Blum, Focal and generalized slowing, coma, and brain death, *The Clinical Neurophysiology Primer*, (Springer, 2007), pp. 127–140.
4. J. W. Britton, L. C. Frey, J. Hopp, P. Korb, M. Koubeissi, W. Lievens, E. Pestana-Knight and E. L. St, *Electroencephalography (EEG): An introductory text and atlas of normal and abnormal findings in adults, children, and infants* (American Epilepsy Society, Chicago, 2016).
5. R. Soikkeli, J. Partanen, H. Soininen, A. Pääkkönen and P. Riekkinen Sr, Slowing of eeg in parkinson’s disease, *Electroencephalography and clinical neurophysiology* **79**(3) (1991) 159–165.
6. N. Kane, J. Acharya, S. Beniczky, L. Caboclo, S. Finnigan, P. W. Kaplan, H. Shibusaki, R. Pressler and M. J. van Putten, A revised glossary of terms most commonly used by clinical electroencephalographers and updated proposal for the report format

of the eeg findings. revision 2017, *Clinical neurophysiology practice* **2** (2017) p. 170.

7. O. Mecarelli, *Clinical electroencephalography* (Springer, 2019).
8. K. Ohoyama, E. Motomura, K. Inui, Y. Nishimura, K. Ushiro, N. Matsushima, M. Maeda, H. Tanii, D. Suzuki, K. Hamanaka *et al.*, Source localization of posterior slow waves of youth using dipole modeling, *Psychiatry and clinical neurosciences* **66**(7) (2012) 582–586.
9. J. S. Doescher, T. J. deGrauw, B. S. Musick, D. W. Dunn, A. J. Kalnin, J. C. Egelhoff, A. W. Byars, V. P. Mathews and J. K. Austin, Magnetic resonance imaging (mri) and electroencephalographic (eeg) findings in a cohort of normal children with newly diagnosed seizures, *Journal of child neurology* **21**(6) (2006) 490–495.
10. A. Aminov, J. M. Rogers, S. J. Johnstone, S. Middleton and P. H. Wilson, Acute single channel eeg predictors of cognitive function after stroke, *PLoS one* **12**(10) (2017) p. e0185841.
11. K. K. Iyer, Effective assessments of electroencephalography during stroke recovery: contemporary approaches and considerations, *Journal of neurophysiology* **118**(5) (2017) 2521–2525.
12. R. Mane, E. Chew, K. S. Phua, K. K. Ang, A. P. Vinod and C. Guan, Quantitative eeg as biomarkers for the monitoring of post-stroke motor recovery in bci and tdc rehabilitation, *2018 40th Annual International Conference of the IEEE Engineering in Medicine and Biology Society (EMBC)*, IEEE2018, pp. 3610–3613.
13. C. Bentes, A. R. Peralta, P. Viana, H. Martins, C. Morgado, C. Casimiro, A. C. Franco, A. C. Fonseca, R. Galdes, P. Canhão *et al.*, Quantitative eeg and functional outcome following acute ischemic stroke, *Clinical Neurophysiology* **129**(8) (2018) 1680–1687.
14. Y. Chen, W. Xu, L. Wang, X. Yin, J. Cao, F. Deng, Y. Xing and J. Feng, Transcranial doppler combined with quantitative eeg brain function monitoring and outcome prediction in patients with severe acute intracerebral hemorrhage, *Critical Care* **22**(1) (2018) p. 36.
15. F. Riaz, A. Hassan, S. Rehman, I. K. Niazi and K. Dremstrup, Emd-based temporal and spectral features for the classification of eeg signals using supervised learning, *IEEE Transactions on Neural Systems and Rehabilitation Engineering* **24**(1) (2015)

- 28–35.
16. S. Finnigan, A. Wong and S. Read, Defining abnormal slow eeg activity in acute ischaemic stroke: Delta/alpha ratio as an optimal qeeg index, *Clinical Neurophysiology* **127**(2) (2016) 1452–1459.
 17. X.-W. Wang, D. Nie and B.-L. Lu, Emotional state classification from eeg data using machine learning approach, *Neurocomputing* **129** (2014) 94–106.
 18. Z. Tang, C. Li and S. Sun, Single-trial eeg classification of motor imagery using deep convolutional neural networks, *Optik* **130** (2017) 11–18.
 19. J. Thomas, L. Comoretto, J. Jin, J. Dauwels, S. S. Cash and M. B. Westover, Eeg classification via convolutional neural network-based interictal epileptiform event detection, *2018 40th Annual International Conference of the IEEE Engineering in Medicine and Biology Society (EMBC)*, IEEE2018, pp. 3148–3151.
 20. O. Tsinalis, P. M. Matthews, Y. Guo and S. Zafeiriou, Automatic sleep stage scoring with single-channel eeg using convolutional neural networks, *arXiv preprint arXiv:1610.01683* (2016).
 21. A. Sors, S. Bonnet, S. Mirek, L. Vercueil and J.-F. Payen, A convolutional neural network for sleep stage scoring from raw single-channel eeg, *Biomedical Signal Processing and Control* **42** (2018) 107–114.
 22. H. Phan, F. Andreotti, N. Cooray, Y. O. Chèn and M. De Vos, Dnn filter bank improves 1-max pooling cnn for single-channel eeg automatic sleep stage classification, *2018 40th Annual International Conference of the IEEE Engineering in Medicine and Biology Society (EMBC)*, IEEE2018, pp. 453–456.
 23. A. Supratak, H. Dong, C. Wu and Y. Guo, Deep-sleepnet: A model for automatic sleep stage scoring based on raw single-channel eeg, *IEEE Transactions on Neural Systems and Rehabilitation Engineering* **25**(11) (2017) 1998–2008.
 24. S. López, I. Obeid and J. Picone, Automated interpretation of abnormal adult electroencephalograms, *MS Thesis, Temple University* (2017).
 25. L. A. Gemein, R. T. Schirrmeister, P. Chrabaszcz, D. Wilson, J. Boedecker, A. Schulze-Bonhage, F. Hutter and T. Ball, Machine-learning-based diagnostics of eeg pathology, *NeuroImage* (2020) p. 117021.
 26. S. Handayani, Y. Diansari, E. Bahar and W. Novantina, Eeg changes in patients with intracranial tumors and seizures symptom at mohammad hoesin hospital Palembang, *Journal of Physics: Conference Series*, **1246**(1), IOP Publishing2019, p. 012014.
 27. A. Harati, M. Golmohammadi, S. Lopez, I. Obeid and J. Picone, Improved eeg event classification using differential energy, *2015 IEEE Signal Processing in Medicine and Biology Symposium (SPMB)*, IEEE2015, pp. 1–4.
 28. I. Obeid and J. Picone, The temple university hospital eeg data corpus, *Frontiers in neuroscience* **10** (2016) p. 196.
 29. J. Thomas, J. Jin, P. Thangavel, E. Bagheri, R. Yuvavaraj, J. Dauwels, R. Rathakrishnan, J. J. Halford, S. S. Cash and B. Westover, Automated detection of interictal epileptiform discharges from scalp electroencephalograms by convolutional neural networks, *International Journal of Neural Systems* (2020).
 30. J. Jing, J. Dauwels, T. Rakthanmanon, E. Keogh, S. Cash and M. Westover, Rapid annotation of interictal epileptiform discharges via template matching under dynamic time warping, *Journal of neuroscience methods* **274** (2016) 179–190.
 31. S. Raschka, *Python machine learning* (Packt Publishing Ltd, 2015).
 32. A. J. Smola and B. Schölkopf, A tutorial on support vector regression, *Statistics and computing* **14**(3) (2004) 199–222.
 33. J. H. Friedman, Stochastic gradient boosting, *Computational statistics & data analysis* **38**(4) (2002) 367–378.
 34. Y. Freund and R. E. Schapire, A decision-theoretic generalization of on-line learning and an application to boosting, *European conference on computational learning theory*, Springer1995, pp. 23–37.
 35. A. Liaw, M. Wiener et al., Classification and regression by randomforest, *R news* **2**(3) (2002) 18–22.
 36. N. V. Chawla, K. W. Bowyer, L. O. Hall and W. P. Kegelmeyer, Smote: synthetic minority over-sampling technique, *Journal of artificial intelligence research* **16** (2002) 321–357.
 37. A. Gulli and S. Pal, *Deep learning with Keras* (Packt Publishing Ltd, 2017).
 38. D. P. Kingma and J. Ba, Adam: A method for stochastic optimization, *arXiv preprint arXiv:1412.6980* (2014).
 39. A. C. Grant, S. G. Abdel-Baki, J. Weedon, V. Arnedo, G. Chari, E. Koziorynska, C. Lushbough, D. Maus, T. McSween, K. A. Mortati et al., Eeg interpretation reliability and interpreter confidence: a large single-center study, *Epilepsy & Behavior* **32** (2014) 102–107.
 40. P. Piccinelli, M. Viri, C. Zucca, R. Borgatti, A. Romeo, L. Giordano, U. Balottin and E. Beghi, Inter-rater reliability of the eeg reading in patients with childhood idiopathic epilepsy, *Epilepsy research* **66**(1-3) (2005) 195–198.
 41. K. Noe, Most experts agree... but what about other eeg readers?, *Epilepsy Currents* **20**(2) (2020) 78–79.
 42. A. M. Saxe, P. W. Koh, Z. Chen, M. Bhand, B. Suresh and A. Y. Ng, On random weights and unsupervised feature learning., *ICML*, **2**(3)2011, p. 6.
 43. A. M. Saxe, J. L. McClelland and S. Ganguli, Exact solutions to the nonlinear dynamics of learning in deep linear neural networks, *arXiv preprint arXiv:1312.6120* (2013).
 44. L. v. d. Maaten and G. Hinton, Visualizing data using t-sne, *Journal of machine learning research* **9**(Nov) (2008) 2579–2605.